RSC Advances

ROYAL SOCIETY OF CHEMISTRY

www.rsc.org/advances

Graphical Abstract

Hydrothermally stable ES40-derived silica matrices with less than 30% pore volume loss are closely associated with a more open silica microstructure formed from thermal consolidation of larger silica particles.

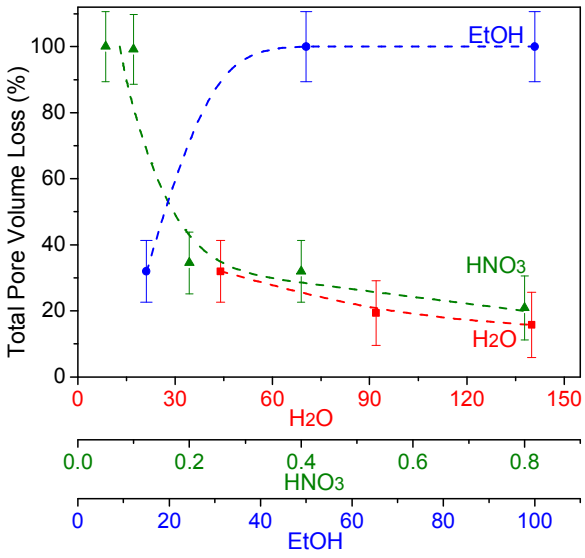

RSC Advances

RSCPublishing

ARTICLE

Improved hydrothermal stability of silica materials prepared from ethyl silicate 40

Cite this: DOI: 10.1039/x0xx00000x

Shengnan Wang[a], David K. Wang[a*], Kevin S. Jack[b], Simon Smart[a], João C. Diniz da Costa[a]

Received 00th January 2012,
Accepted 00th January 2012

DOI: 10.1039/x0xx00000x

www.rsc.org/advances

Microporous silica materials with improved hydrothermal stability were synthesized through a sol-gel process using ethyl silicate 40 as the starting silica precursor. The effects of reactants for water (hydrolysing agent), acid (catalyst) and ethanol (solvent) ratios on the microstructure of the silica matrices and their hydrothermal stability under harsh conditions (550 °C, 75 mol% vapour, 20 h) were systemically studied. All the calcined silica matrices were microporous and the degree of microporosity was found to increase with decreasing water and acid ratios, or increasing ethanol ratio. The most hydrothermally stable matrix was obtained by promoting the water and acid ratios whilst decreasing the ethanol ratio. A strong correlation was found between the FTIR area ratio of silanol/siloxane vibrational peaks and the initial micropore volume, and this relationship revealed that the greatest pore volume loss (> 70%) occurred in the xerogels possessing high silanol/siloxane ratio (> 0.16) and high initial micropore percentage (> 85%). SAXS data also revealed that the most robust, hydrothermally stable silica matrices are closely associated with the formation of a more open silica microstructure derived from thermal consolidation of larger silica particles.

1 Introduction

Silica porous materials have been widely applied in catalysis, adsorption, sensor, and molecular sieving membranes materials.[1-4] These materials are typically prepared via the conventional sol-gel methods, in which an alkoxysilane precursor undergoes hydrolysis and condensation reactions in the presence of a mineral acid or base catalyst to produce a silica matrix. Tetraethyl orthosilicate (TEOS) has been extensively investigated, due to the ease of processing and good control of physicochemical properties offered by this silica precursor. However, a major potential downside of this approach is that the structural integrity of microporous silica matrices is generally compromised under water vapour exposure.[5-9] The issue here is that the surface functional groups responsible for the formation of microporous silica networks (i.e. silanols groups (Si-OH)), are also responsible for the hydrothermal instability.

They attract water molecules to adsorb to the surface which reacts (by hydrolysis) with the neighboring siloxane backbone. This process creates unconstrained mobile silanol species, which migrate within the silica matrix to minimize the surface energy of the pore network by filling in the small pores.[10, 11] As a result of the restructuring and recondensation, the silica matrices densify which leads to a significant loss of selectivity and functionality.To address this problem, several strategies have been reported to obtain hydrothermally stable silica materials namely: (i) post-synthesis hydrothermal treatment as a pre-emptive process aimed at reducing the concentration of available silanol species;[12] (ii) incorporation of another ceramic component for example using Ti, Al or Zr to form Si–O–M bonds (M; metal), which are less susceptible to hydrolysis;[13, 14] (iii) increasing surface hydrophobicity by embedding carbon groups using organosilica precursors,[15-18] which include terminal alkyl groups, such as $\equiv$Si–CH_3 or organic bridges, such as Si–CH_2–CH_2–Si in their structure, or by post-synthesized silylation; and iv) by doping with metal/carbon particles to limit silanol migration and reconstruction.[11, 19-21] It has also been reported that silica matrices modified by the incorporation of inorganic salts during the sol-gel synthesis process not only produce an improved hydrothermal stability but also a thicker pore walls leading to a better structural integrity.[22, 23] A considerable drawback of these strategies is the use of relatively expensive organosilica precursors, secondary component and/or additional post-treatment.

[a]The University of Queensland, FIMLab – Films and Inorganic Membrane Laboratory, School of Chemical Engineering, Brisbane, Qld 4072 Australia; [b]The University of Queensland, Centre for Microscopy and Microanalysis, Brisbane, Qld 4072 Australia

[*] corresponding author: d.wang1@uq.edu.au

Tel.:+61 7 3365 9760 Fax: +61 7 3365 4199

Electronic Supplementary Information (ESI) available: See DOI: 10.1039/b000000x/

In this work, we propose another alternative strategy to produce a more stable silica structure by using ethyl silicate 40 (ES40) as the silica precursor of choice instead of TEOS. ES40 is a partially-condensed TEOS oligomer composed of 40% of the silica by mass. ES40 is also commercially available and is lower in cost compared to the TEOS precursor. Although ES40-derived silica materials have not been fully explored, ES40 has generally been employed in the preparation of mesoporous materials.[24-27] For examples, mesoporous silica xerogels and aerogels using ES40 had shown to produce a low concentration of silanol groups[27] and ES40-derived MCM-41 exhibited a higher wall thickness than that of the TEOS counterpart, leading to a higher thermal stability.[24] Recently, Miller and co-workers pioneered the preparation of ultra-microporous ES40-derived materials combined with cobalt oxide.[28] Subsequently, Wang et al.[29] showed for the first time that ES40 could also be used for the preparation of microporous silica/cobalt oxide by rapid thermal treatment which could not be realized using the TEOS precursor. Hence, ES40 has demonstrated potential as a precursor in the synthesis of hydrostable microporous materials due to its improved structural stability.

Based on a limited number of studies into ES40-derived materials, the sol-gel conditioning of ES40-based microporous materials without any additives, specifically the effect of sol-gel ratios on the structural formation and hydrothermal stability, remains unexplored. Therefore, this work investigates the hydrothermal effect of ES40 derived materials. Of particular importance, many industrial processes require microporous materials for processing gas streams containing water vapour. To this end, this work studies the effects of sol-gel synthesis conditions, including different ethanol, acid catalyst and water ratios, on the structural formation and chemical properties. The hydrothermal stability of the resultant ES40 xerogels is also investigated using a harsh hydrothermal treatment condition (550 °C, 75 mol% vapour, 20 h).

2 Experimental

2.1 Sol-gel Synthesis

Table 1. Molar ratios of the reactants used in the sol-gel process.

Sample Code*	Si	EtOH	H_2O	HNO_3
H_2O-44	4	15	**44**	0.4
H_2O-92			**92**	
H_2O-140			**140**	
HNO_3-0.05	4	15	44	**0.05**
HNO_3-0.1				**0.1**
HNO_3-0.2				**0.2**
HNO_3-0.4				**0.4**
HNO_3-0.8				**0.8**
EtOH-15	4	**15**	44	0.4
EtOH-50		**50**		
EtOH-100		**100**		

* Samples are named as N-y, where N is the name of the varying component (H_2O, HNO_3 or EtOH) and y is the molar ratio of N component.

The sol-gel procedure to produce microporous materials was adopted from Miller and co-workers.[28] Briefly 1 M nitric acid (HNO_3), distilled water and ethanol (EtOH, AR grade) were mixed briefly followed by dropwise addition of ES40 (Colcoat Co., Japan) into the solution under stirring in an ice bath. The mixture was stirred for 10 min and then the sols were dried in an oven at 60 °C for over 4 days. Subsequently, the dried gels were ground into powders and calcined in air at 630 °C for 2.5 h with a ramp up and down rate of 1 °C min^{-1} to obtain the resultant xerogel samples for material characterization and hydrothermal treatment. The final molar ratios ($ES40:EtOH:H_2O:HNO_3$) of the sol compositions are listed in Table 1. The molar ratio of H_2O was altered from 44 to 140, HNO_3 from 0.05 to 0.8 and EtOH from 15 to 100 respectively to study the effect of these three reactant components.

2.2 Hydrothermal test

Hydrothermal stability was evaluated by exposing the xerogels to harsh conditions of 75 mol% vapor at 550 °C for 20 h with a ramp up and down rate of 5 °C min^{-1}. As shown in Fig. 1, the flow rate of carrier nitrogen gas was set to 40 mL min^{-1} by a flow meter and the rate of water was set to 5.4 g h^{-1} by liquid flow controller, both of which were mixed and heated to 200 °C in a vaporizer to produce 75 mol% vapour. The vapour continuously flowed through a quartz tube furnace controlled by a PID temperature controller. The xerogel samples were placed in the middle of the quartz tube.

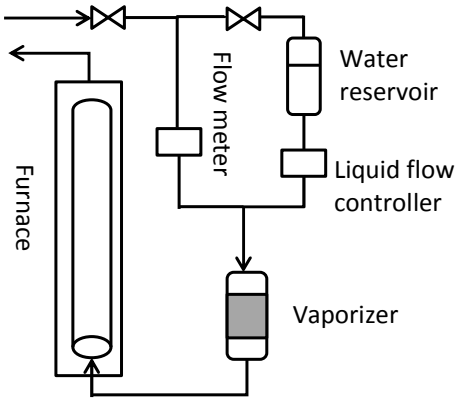

Fig. 1 Schematic diagram for the hydrothermal treatment set up.[30]

2.3 Material Characterizations

Fourier transform infra-red (FTIR) characterization was performed by a Shimadzu IRAffinity-1 with a Pike MIRacle diamond attenuated total reflectance (ATR) attachment. The spectra were collected over a wavenumber range of 1400–600 cm^{-1}. Peak deconvolution of the silanol (960 cm^{-1}) and siloxane (1050 cm^{-1}) vibrations was performed using the Fityk program. Both peak positions and height were allowed to vary between samples to achieve the best possible fit. Half width half max parameter was fixed for each peak across all the samples. The intensity of siloxane peak was normalized to 100% for each spectrum. Cross-polarisation magic-angle-spinning (CP/MAS) solid-state ^{29}Si nuclear magnetic resonance spectroscopy (NMR) was performed on an Avance III spectrometer (Bruker) for silicon groups. Nitrogen adsorption was performed at -196 °C by a Micromeritics TriStar 3000. Prior to each measurement, samples were degassed at 200 °C overnight. The specific surface area was calculated from the adsorption isotherms by the Brunner-Emmett-Teller (BET) method and total pore volume was determined from the data point at ~0.95 P/P_o. The pore size distributions were calculated by using Density Functional Theory (DFT) method applied to the whole adsorption branch of the isotherms using the model of cylindrical pores in oxide surfaces. Small-angle X-ray scattering (SAXS) was measured on an Anton Paar SAXSess

instrument which employs an anode source (Cu Kα radiation at 40 kV and 35 mA), a CCD detector and a line-focus (Kratky) geometry. Samples of fine powders were measured between thin polymer films at room temperature and the resultant data were reduced to remove the background scattering and detector dark current.

3 Results and discussion

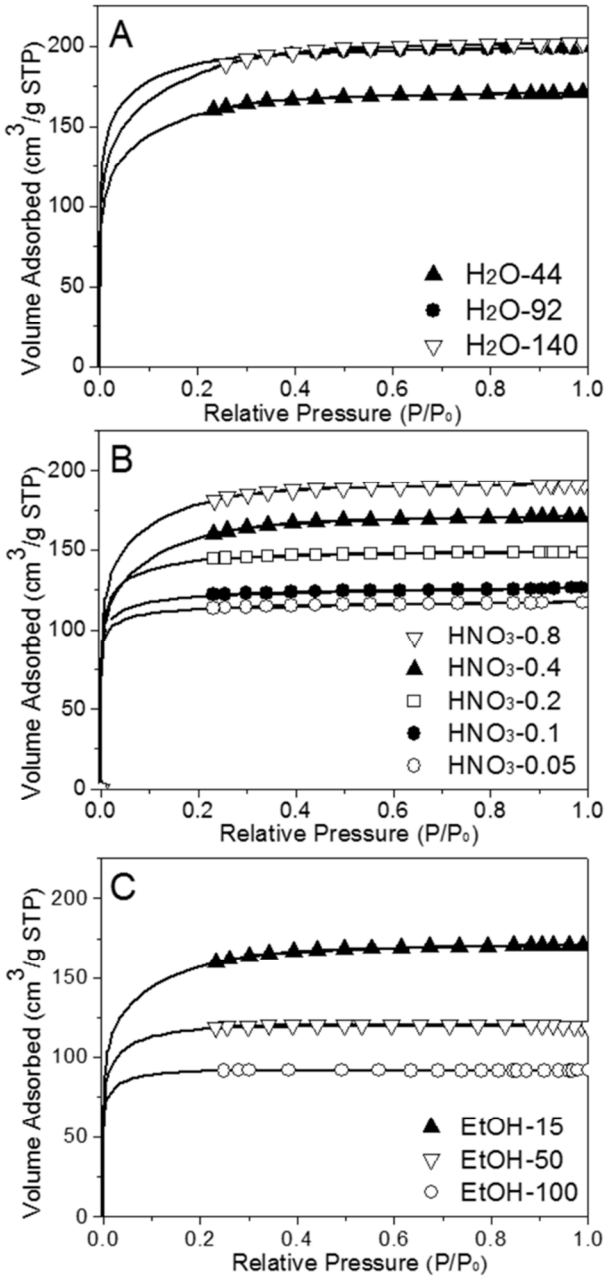

Fig. 2 N_2 adsorption (solid line) and desorption (symbols) isotherms of silica xerogels prepared with different ratio of H_2O (A), HNO_3 (B) and EtOH (C) to Si, respectively.

3.1 Nitrogen Sorption

Three series of sol-gel ES40-derived silica xerogels were prepared by parametrically changing the feed ratios of H_2O, HNO_3 and EtOH as listed in Table 1, and their textural properties were studied by N_2 sorption. Fig. 2 shows the nitrogen adsorption-desorption isotherms of the resultant xerogels. It can clearly be seen that all the isotherms are Type I without any hysteresis, which is characteristic of microporous materials. However, the isotherm profiles of the individual series of silica xerogels consistently changes with increasing or decreasing the sol-gel ratios. For example, the relative pressure at which adsorption saturation plateaus and the amount of volume adsorbed increases with increasing H_2O and HNO_3 ratios, indicating higher total pore volume and surface area.

In comparison increasing the EtOH ratio has the opposite effect. These trends are clearly reflected by the total pore volume as shown in Fig. 3. The total pore volumes increase from 0.18 to 0.30 $cm^3\ g^{-1}$ for the HNO_3-0.05 and HNO_3-0.8 samples respectively. Similarly, the BET surface areas (see Supporting Information Fig. S1) increase from 380 to 617 $m^2\ g^{-1}$ with increasing HNO_3 ratio. The same trend is also observed for the samples in the H_2O series, but conversely for the EtOH sample series. Interestingly, the EtOH-100 xerogel samples exhibit the lowest total pore volume and BET surface area of all samples investigated. This is directly attributed to the dilutive effect of the EtOH solvent on the ES40 hydrolysis and condensation reactions which are expected to be slowed down in EtOH excess.[31] Based on these results, by changing the initial sol-gel reactant ratios, the final textural properties and xerogel pore volumes can be easily controlled with a high degree of reproducibility and fidelity.

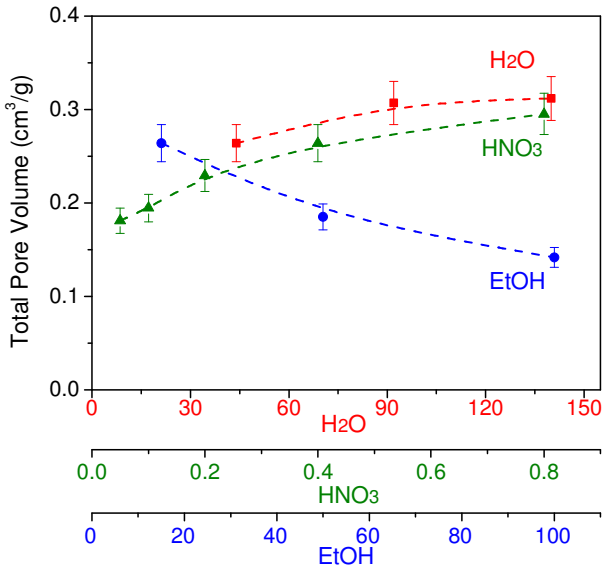

Fig. 3 Total pore volume of silica xerogels prepared from different ratio of H_2O (red ■), HNO_3 (green ▲) and EtOH (blue ●) to Si, respectively.

To examine the hydrothermal stability of the as-synthesized ES40 silica microstructure, xerogel samples were heated to 550 °C for 20 h in the presence of 75 mol% steam vapour. The structural integrity of these samples was determined from the calculated loss of total pore volume before and after hydrothermal treatment. The results are summarized in Fig. 4. It can clearly been seen that xerogel samples with less than 40% loss in total pore volume were prepared by a relatively high H_2O or HNO_3 ratios and low EtOH ratio. For example, the H_2O

series produced a small amount of pore volume loss (15%–32%), particularly in the H_2O-92 and 140 samples. Similarly, when the HNO_3 ratio is greater than 0.2, the hydrothermal stability of the xerogels greatly improved. By contrast, increasing the EtOH ratio beyond 15 profoundly increases the pore volume loss such that the samples are observed to become almost non-porous. These trends exhibited by the three series of xerogels are also in good accord with the results of BET surface area loss after hydrothermal treatment (not shown), as pore volumes are linearly proportional to surface areas.

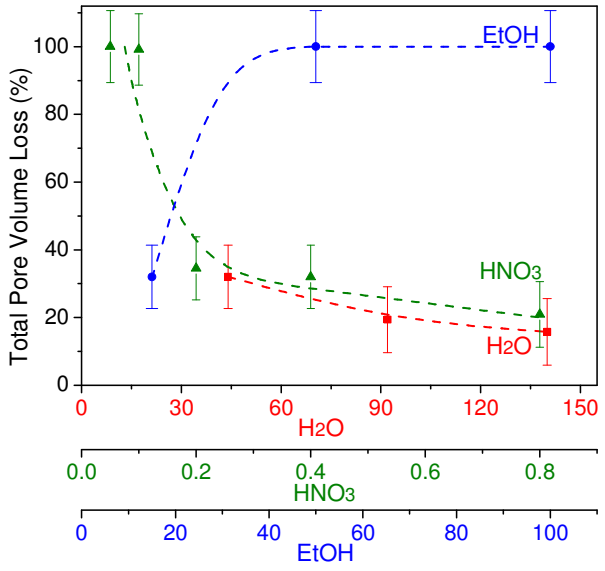

Fig. 4 Total pore volume loss of silica xerogels prepared from different ratio of H_2O (red ■), HNO_3 (green ▲) and EtOH (blue ●) to Si, respectively.

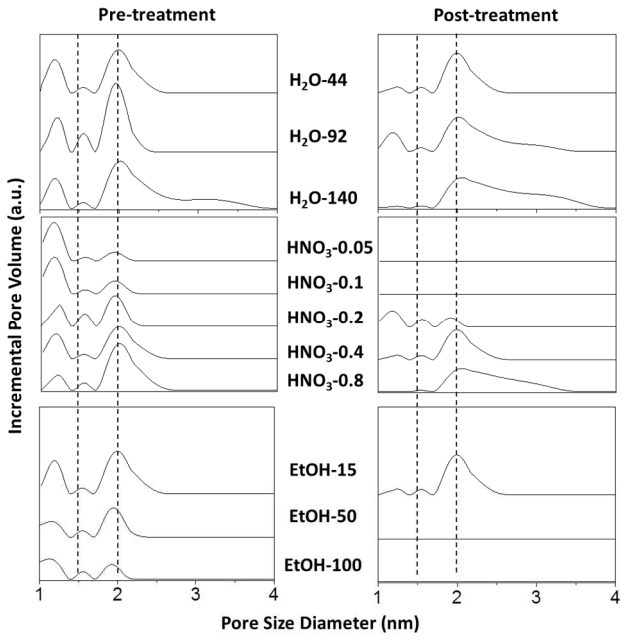

Fig. 5 DFT pore size distribution of the xerogels before and after hydrothermal treatment. The broken lines are guidelines only for pore sizes of 1.5 and 2.0 nm.

Hydrothermal densification of the microporous silica is further qualitatively discussed by the change in pore size distribution as displayed in Fig. 5, which shows the DFT pore size distribution before and after hydrothermal treatment. By comparing the incremental pore volume of the xerogels pre-and post-treatment, the distribution curves either significantly decreased in volume or shifted to high pore diameters after treatment. Where xerogel samples completely densified (e.g. HNO_3-0.05, -0.1, and EtOH-50, -100), the pore size distribution curve became a flat line, implying the closure of pores. In the other cases, the profiles of stable samples showed a shift towards a larger pore size distribution. On closer inspection, these samples seemed to have widened the mesopores (2–4 nm) at the expense of micropore closure (< 2 nm). This means that the hydrothermal treatment imposed on these series of xerogels caused a significant loss of the observed micropores and/or micropore narrowing which may be too small to be accessed by N_2.

It is worthy to mention that by increasing the H_2O and HNO_3 ratios, the distribution profiles of the samples without hydrothermal treatment show an increasing proportion of pore size towards a mesoporous domain which enlarges upon hydrothermal exposure (post treatment), which in turn resisted pore densification. Meanwhile, by increasing the EtOH ratio, the distribution and the trend are reversed. Similar observations were also reported for ordered mesoporous silica materials, of which the micropores were collapsed first followed by partial blocking of the mesopores via acid stability testing.[32] The behavior of hydrothermal densification of silica xerogels is consistent with the previous works on bulk porous silica[11, 33-35] in that the mobile silica generated by hydrothermal treatment prefer to migrate from the larger pores towards the smaller pores to minimise the overall silica surface energy. Thus after recondensation reactions, the smaller pores are closed while larger pores are widened, leading to a loss in porosity in the microporous region.

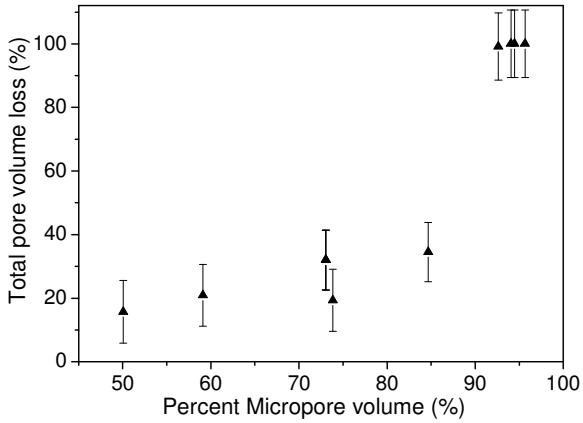

Fig. 6 Total pore volume loss of the hydrothermally treated xerogels as function of percent micropore volume (%) of the as-synthesized silica xerogels before hydrothermal test.

Since the initial micropore content (d_p < 2 nm) of the pre-treated samples leading to the majority of pore closure is directly attributed to hydrothermally unstable matrices, this relationship is further examined. The micropore content is determined from fraction of the cumulative pore volume attributed to pore size below 2 nm based on the DFT pore size distribution. Fig. 6 shows the micropore volume percentage of

the pre-treated samples against the total pore volume loss. At a first glance, the samples with an initial micropore volume larger than 85% (highly microporous) became completely dense after hydrothermal test, while the other samples having lower micropore volume preserved their total pore volume to varying degrees. Therefore, it can be deduced that hydrothermal stability of these silica xerogels is closely correlated to the initial micropore volume which can be simply controlled by changing the feed reactant ratios during the sol-gel process.

3.2 FTIR and CP/MAS ^{29}Si NMR Spectroscopies

Another important aspect of thermal consolidation of microporous silica matrices is the chemical and molecular properties which can be probed by FTIR-ATR technique readily. Fig. S2 shows the FTIR spectra of the three series of calcined xerogel samples in the range from 1400 to 600 cm^{-1}, where the peak at ~960 cm^{-1} is assigned to the vibration of the silanol bonds and the major peak at ~1050 cm^{-1} is assigned to the stretching vibrations of the siloxane bonds. The latter also shows various bands near 800, 1090 and 1160 cm^{-1} associated with various symmetric and anti-symmetric Si-O-Si vibrations which arise from highly condensed siloxane ring species.[29, 36, 37] In order to provide a semi-quantitative analysis of the chemical compositions, the peak at ~1050 cm^{-1} is normalized for all the spectra and these peaks were deconvoluted with a special attention given to the silanol band at 960 cm^{-1} and the siloxane band at 1050 cm^{-1} according to a previously reported methodology.[29, 30]

Fig. 7 shows the area ratio analysis of the bands 960 cm^{-1}/1050 cm^{-1} which allows a comparison of the degree of condensation between the different sample series; where a high ratio corresponds to a high silanol concentration and vice versa. There is a strong correlation between the area ratio and the reactant sol-gel ratios. It can be seen that the concentration of the silanols is significantly promoted by low HNO_3 ratio (< 0.2) or high EtOH ratio (> 15). As mentioned earlier, a high concentration of silanol species can lead to an unstable silica structure. This is evidenced by the similarity in results between Fig. 7 and the hydrothermal densification as shown in Fig. 4.

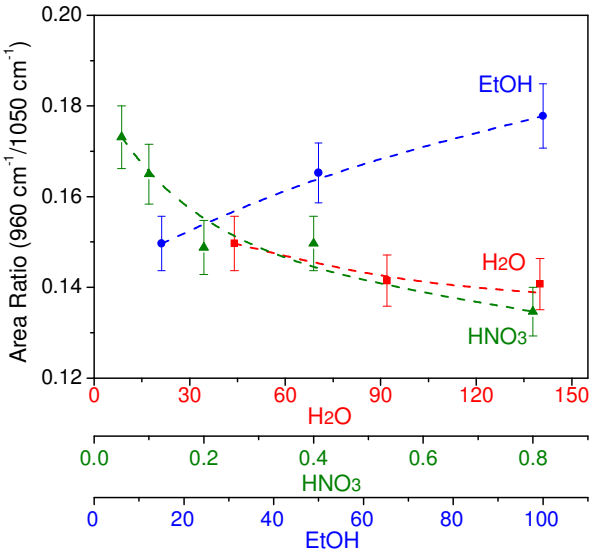

Fig. 7 Comparative FTIR ratios of silanol to siloxane of silica xerogels prepared from different ratios of H_2O (red ■), HNO_3 (green ▲) and EtOH (blue ●) to Si, respectively.

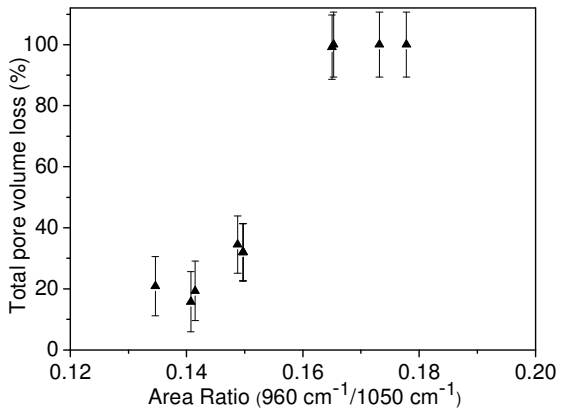

Fig. 8 Total pore volume loss of silica xerogels as function of comparative silanol/siloxane area ratio.

Microporous silica surfaces possess an abundance of hydrophilic silanol groups which attract water molecules to the material surface. This initiates a cascade reaction of siloxane hydrolysis which undergo bond cleavage and silanol formation. The as-formed silanols become mobile moving to minimize the surface energy by migrating towards to the small micropores where they further crosslink and reform the siloxane network. This process eventually closes the small micropores. This migration of the mobile silanol groups concurrently causes the larger pores to widen. This mechanism has been reported by Duke et al.[11] and is supported in this study.

Fig. 8 shows the total pore volume loss of the xerogels as function of the same peak area ratios irrespective of the reactant ratios. One can clearly observe that the results can be separated into two groups. Silica matrices with a relatively higher silanol concentration (area ratio > 0.16) completely collapsed after the hydrothermal treatment. By contrast, the group with a lower total pore volume loss inherently possesses a lower silanol concentration. This further suggests that hydrothermal stability of the silica microstructure in this work is related to the presence of these silanol species with a ratio threshold of 0.16, which is a semi-quantitative correlation.

Incidentally, these results also point towards a correlation between the FTIR peak area ratio and the micropore volume (Fig. 6) whereby both trends of the pore volume loss demonstrate in FTIR area ratios of silanol to siloxane vibrational peaks the region of high silanol ratio (> 0.16) and high initial micropore percentage (> 85%). This indicates that the probability of hydrothermal densification of the silica matrices is greatly increased in a more microporous sample with higher silanol content. In a similar vein, Zhao and co-workers[9, 38, 39] have reported that the surface of micropores of silica matrix possess an abundance of silanol groups, which preferentially condense upon hydrothermal treatment over the mesopores. Therefore, based on these observations, hydrothermal stability of these series of microporous silica xerogels is intrinsically linked to the physical and chemical properties which can be easily controlled by changing the reactant ratios.

Furthermore, the evolution of the silica structure can be further confirmed by the structural transition of the silanol to siloxane groups based on the comparative CP/MAS ^{29}Si NMR quantification of the Q^n species populations before and after hydrothermal treatment. The results of the ^{29}Si NMR spectra of the H_2O-44 and H_2O-140 xerogels samples are shown in Fig.

S3 (supporting information). By peak deconvolution, the percent variation of the Q^n species of the pre-and post-treatment silica samples is shown in Fig. 9. Both samples show an increase in Q^4 population after treatment, at the cost of Q^2 and Q^3, illustrating restructuring of silanols to siloxanes. However, the increase in the Q^4 species as a result of loss of Q^3 is larger for the H_2O-44 samples indicating further silanol condensation took place, which is in good agreement with the total pore volume loss of the H_2O-44 samples (32%) being twice as much as that of the H_2O-140 samples (15%). These findings are also consistent with the previous reports by Duke et al.[11] and Liu et al.,[30] who also observed that an increase of the Q^4 species after treatment is more pronounced in the more unstable silica samples than the stable ones. Nevertheless, these reports only demonstrated that the modified silica matrices with carbon[11] and cobalt oxide[30] are stable, whereas that the pure silica matrices are completely dense after hydrothermal treatment.

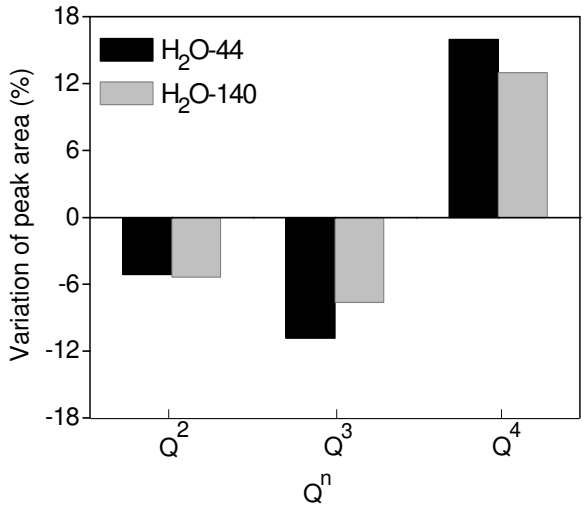

Fig. 9 Percentage variation of the deconvoluted peak area of Q^n species between the as-synthesized and the treated xerogels (H_2O-44 and H_2O-140).

3. 3 SAXS Measurements

The further shed more light into the microstructure of the calcined silica xerogels, these powders were further investigated by SAXS. Fig. 10A and B show the forward scattering presented as $(I(q)\times q^3)$ as a function of q (where q is the wavevector and I(q) is the measured, line-focused, scattered intensity at q) for the HNO_3-0.05 and HNO_3-0.8 as-synthesized xerogel powder samples, respectively. These two samples in the HNO_3 series were selected as representative samples for each of the hydrothermally weak and stable silica matrices. In both of the SAXS profiles, the presence of a plateau can be seen at relatively higher q values, indicating the onset of the Porod scattering region in the SAXS profile of the powder. This Porod scattering indicates that the powder is comprised of well-defined smooth surfaces, i.e. the gels consist of a well-dispersed homogenous silica microstructure and is consistent with the SAXS typically reported for silica gels.[26, 27]

Moreover, it can be seen in Fig. 10 that the value of q at the onset of the plateau (q_c) is greater for the HNO_3-0.05 sample (4.3 nm^{-1}) compared with the HNO_3-0.8 sample (2.3 nm^{-1}). Indeed the mean radius of the primary silica particles can be approximated from these onset values: $r_0 \approx \pi/q_c$.[40] The silica particles (r_0) of the HNO_3-0.8 sample are, therefore, estimated to be twice as large as that of the HNO_3-0.05 xerogel sample. Thus, it is hypothesized that the thermal consolidation of silica particles in the HNO_3-0.8 xerogel sample creates a relatively larger average pore sizes and total pore volume as shown in the schematics of Fig. 10. Such hypothesis is consistent with the larger total pore volume (Fig. 3) and DFT pore size distributions (Fig. 5) derived from N_2 sorption analysis.

Based on these results, the microstructure of the HNO_3-0.8 xerogel sample with a larger pore volume and pore size conferred a better structural integrity as evidenced by a total pore volume

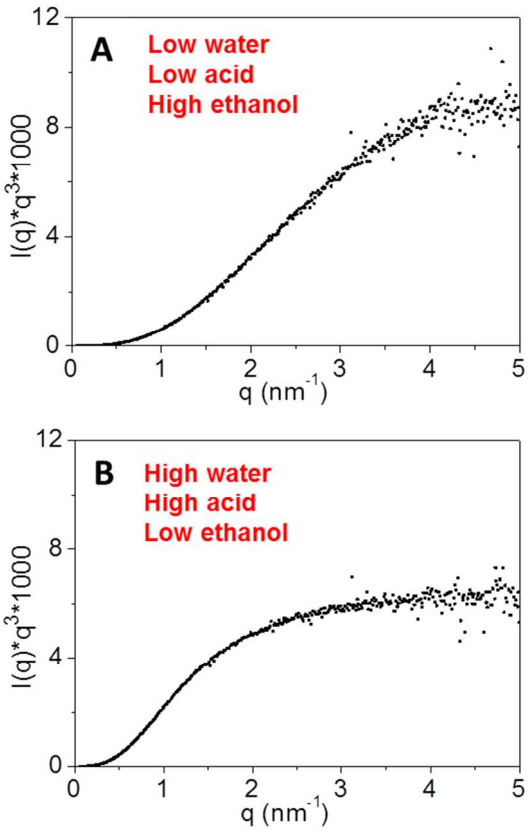

Fig. 10 SAXS profiles of the as-synthesized HNO_3-0.05 (A) and HNO_3-0.8 (B) xerogel powder samples.

loss (<30 %) being significantly lower than that of the HNO_3-0.05 sample (>70%). Therefore, the improved hydrothermal stability of silica matrices obtained by the controlled sol gel conditions in this work (higher H_2O, HNO_3 ratios and lower EtOH ratio) is attributed to the formation of a more robust, open silica microstructure condensed by larger silica particles on one hand and a lower proportion of silanol groups in the matrix on the other.

3. 4 Sol-Gel Process

By comparing the silica xerogels made from the different reactant ratios, it can be deduced that the use of higher H_2O, HNO_3 ratios and lower EtOH ratio during the sol-gel process can produce a silica matrix with larger pore volume and better hydrothermal stability. It is clear that these properties are attributed to the formation and subsequent packing of larger

silica particles. As water is the main reactant responsible for hydrolysis reaction in the sol gel process, a low H_2O ratio demotes the hydrolysis and condensation reactions. In this case, hydrolysis is more inclined to proceed via the most basic Q^1 species on the ES40 molecules due to a lower steric hindrance. As can be expected, the reactive hydrolyzed sites which allow the condensation to propagate (polymerization) are primarily located at the chain ends where reaction is spatially limited, hence forming smaller silica particles. This process is anticipated to form a better packing density of the final silica matrices with more silanol groups, which is reflected by a more microporous texture (Fig. 2) with a significantly lower total pore volume (Fig. 3).

On the other hand, high H_2O ratio can promote hydrolysis and thus produce more reactive sites from the Q^1 species as well as the more acidic Q^2 species on the pendant groups of the ES40 molecules. As a consequence, fast chain-to-chain random polymerization due to a higher statistical crosslinking is expected. Such a process also promotes a tendency to form clusters leading to a much larger silica particles and more open microstructure with relatively lower silanol groups. Similar trends have also been reported for sol-gel derived cobalt oxide silica systems by Wang et al.[29] by using the ES40 precursor. Therefore, during the hydrothermal treatment, the silica network is firmly supported by the more robust, larger silica particles which resisted densification.

Similarly, increasing the HNO_3 ratio also promotes the sol-gel process due to its catalytic effect. All of the initial sol systems in this work had a measured pH value of around 1 except for the HNO_3-0.05 sample, which was near 2. In the acidic conditions, when pH is significantly lower than the point of zero charge (~2) of silica polymeric particles,[41] the sol-gel reactions rapidly proceeds through the protonated alkoxide group ($SiORH^+$) during the hydrolysis and protonated silanol groups ($SiOH_2^+$) during the condensation reactions.[31] Protonation of these groups makes the silicon atom more electrophilic and thus more reactive towards water or silanol species. This would lead to a faster hydrolysis and condensation reactions causing larger silica particles to form in the system as evidenced by the SAXS results.

On the contrary, excess ethanol retards the hydrolysis process by favoring the reverse reaction since it is a by-product of the sol-gel process. Moreover, by increasing the ethanol concentration, the sol solution is significantly diluted resulting a diffusion-limited polymerization process with a longer gelation time.[31, 42] Essentially, the resultant xerogel is formed by smaller polymeric particles with higher silanol species present in the silica matrix, hence leading to a more microporous texture and a weaker microstructure.

Conclusions

Microporous molecular sieving silica xerogels with improved hydrothermal stability are prepared by using ES40 as silica precursor. The effects of synthesis conditions, including water (hydrolysing agent), acid (catalyst) and ethanol (solvent) ratios on the structure properties and hydrothermal stability of the resultant xerogels are systemically studied. All silica xerogels were found to possess a Type I microporous texture, but the degree of microporosity (pore volume, pore size, and pore size distribution) can be finely controlled by changing these ratios. Highly microporous silica matrices were promoted by low water and acid ratios, or high ethanol ratio in this work. By exposing xerogels to harsh conditions (550 °C, 75 mol% vapour, 20 h), the most hydrothermal stable matrix with a minimum total pore volume reduction of 15% was obtained by adjusting the ratio of water to 140, acid to 0.4 and ethanol to 15. A correlation between the FTIR area ratio of silanol/siloxane vibrational peaks and the micropore volume revealed that the greatest pore volume loss (> 70%) occurred in the region of high area ratio (> 0.16) and high initial micropore percentage (> 85%). SAXS data also revealed that the improved hydrothermal stability of the microporous silica material is attributed to the formation of a more robust, open silica microstructure condensed by larger silica particles on one hand and a lower proportion of silanol groups in the matrix on the other. This work paves ways for a simple sol-gel synthesis of structurally stable microporous silica matrices with predictable physicochemical properties that are desired for a variety of technological applications, such as catalysis, adsorption, sensor, and molecular sieving membranes materials.

Acknowledgements

The authors would like to acknowledge funding support from the Australian Research Council through Discovery Project Grant DP140102800. Shengnan Wang also acknowledges funding support from The University of Queensland in providing a UQ International Scholarship. The authors acknowledge the facilities, and the scientific and technical assistance, of the Australian Microscopy & Microanalysis Research Facility at the Centre for Microscopy and Microanalysis. J. C. Diniz da Costa gratefully thanks the support given by the ARC Future Fellowship Program (FT130100405).

References

1. C. Yacou, S. Smart and J. C. Diniz da Costa, *Energ. Environ. Sci.*, 2012, 5, 5820-5832.
2. E. L. Margelefsky, R. K. Zeidan and M. E. Davis, *Chem. Soc. Rev.*, 2008, 37, 1118-1126.
3. S. K. Parida, S. Dash, S. Patel and B. K. Mishra, *Adv. Colloid Interface Sci.*, 2006, 121, 77-110.
4. W. Yang, P. J. Lopez and G. Rosengarten, *Analyst*, 2011, 136, 42-53.
5. K. Cassiers, T. Linssen, M. Mathieu, M. Benjelloun, K. Schrijnemakers, P. Van Der Voort, P. Cool and E. F. Vansant, *Chem. Mater.*, 2002, 14, 2317-2324.
6. G. R. Gallaher and P. K. T. Liu, *J. Membr. Sci.*, 1994, 92, 29-44.
7. G. R. Gavalas, C. E. Megiris and S. W. Nam, *Chem. Eng. Sci.*, 1989, 44, 1829-1835.
8. H. Imai, H. Morimoto, A. Tominaga and H. Hirashima, *J. Sol-Gel Sci. Technol.*, 1997, 10, 45-54.
9. F. Zhang, Y. Yan, H. Yang, Y. Meng, C. Yu, B. Tu and D. Zhao, *J. Phys. Chem. B*, 2005, 109, 8723-8732.
10. R. K. Iler, *The chemistry of silica : solubility, polymerization, colloid and surface properties, and biochemistry*, Wiley, New York, 1979.
11. M. C. Duke, J. C. Diniz da Costa, D. D. Do, P. G. Gray and G. Q. Lu, *Adv. Funct. Mater.*, 2006, 16, 1215-1220.
12. L. Chen, T. Horiuchi, T. Mori and K. Maeda, *J Phys Chem B*, 1999, 103, 1216-1222.
13. G. P. Fotou, Y. S. Lin and S. E. Pratsinis, *J. Mater. Sci.*, 1995, 30, 2803-2808.
14. S. Araki, Y. Kiyohara, S. Imasaka, S. Tanaka and Y. Miyake, *Desalination*, 2011, 266, 46-50.

15. M. Selvi, M. R. Vengatesan, S. Devaraju, M. Kumar and M. Alagar, *RSC Adv.*, 2014, 4, 8446-8452.
16. R. M. de Vos, W. F. Maier and H. Verweij, *J. Membr. Sci.*, 1999, 158, 277-288.
17. D.-H. Park, N. Nishiyama, Y. Egashira and K. Ueyama, *Ind. Eng. Chem. Res.*, 2001, 40, 6105-6110.
18. Q. Wei, Y.-L. Wang, Z.-R. Nie, C.-X. Yu, Q.-Y. Li, J.-X. Zou and C.-J. Li, *Microporous and Mesoporous Mater.*, 2008, 111, 97-103.
19. N. Coustel, F. Di Renzo and F. Fajula, *J. Chem. Soc., Chem. Commun.*, 1994, DOI: 10.1039/C39940000967, 967-968.
20. D. Zhao, J. Feng, Q. Huo, N. Melosh, G. H. Fredrickson, B. F. Chmelka and G. D. Stucky, *Science*, 1998, 279, 548-552.
21. G. Olguin, C. Yacou, S. Smart and J. C. Diniz da Costa, *RSC Adv.*, 2014, 4, 40181-40187.
22. J. M. Kim, S. Jun and R. Ryoo, *J Phys Chem B*, 1999, 103, 6200-6205.
23. J. Yu, J.-L. Shi, H.-R. Chen, J.-N. Yan and D.-S. Yan, *Microporous and Mesoporous Mater.*, 2001, 46, 153-162.
24. T. R. Gaydhankar, V. Samuel, R. K. Jha, R. Kumar and P. N. Joshi, *Mater. Res. Bull.*, 2007, 42, 1473-1484.
25. T. R. Gaydhankar, U. S. Taralkar, R. K. Jha, P. N. Joshi and R. Kumar, *Cataly. Commun.*, 2005, 6, 361-366.
26. J. Mrowiec-Bialon and A. B. Jarzebski, *Microporous and Mesoporous Mater.*, 2008, 109, 429-435.
27. J. Mrowiec-Bialon, A. B. Jarzebski, L. Pajak, Z. Olejniczak and M. Gibas, *Langmuir*, 2004, 20, 10389-10393.
28. C. R. Miller, D. K. Wang, S. Smart and J. C. Diniz da Costa, *Sci. Rep.*, 2013, 3, 1-6.
29. D. K. Wang, J. C. Diniz da Costa and S. Smart, *J. Membr. Sci.*, 2014, 456, 192-201.
30. L. Liu, D. K. Wang, D. L. Martens, S. Smart, E. Strounina and J. C. Diniz da Costa, *RSC Adv.*, 2014, 4, 18862-18870.
31. C. J. Brinker and G. W. Scherer, *Sol-gel science: the physics and chemistry of sol-gel processing*, Academic Press, Boston, 1990.
32. S. El Mourabit, M. Guillot, G. Toquer, J. Cambedouzou, F. Goettmann and A. Grandjean, *RSC Adv.*, 2012, 2, 10916-10924.
33. R. O. Fournier and J. J. Rowe, *Am. Mineral.*, 1977, 62, 1052-1056.
34. R. Leboda, E. Mendyk, A. Gierak and V. A. Tertykh, *Colloids Surf., A*, 1995, 105, 181-189.
35. R. Leboda, E. Mendyk, A. Gierak and V. A. Tertykh, *Colloids Surf., A*, 1995, 105, 191-197.
36. I. Halasz, M. Agarwal, R. Li and N. Miller, presented in part at the 8th International Symposium on the Characterisation of Porous Solids, Great Britain, 2009.
37. P. Innocenzi, *J. Non-Cryst. Solids*, 2003, 316, 309-319.
38. Q. Li, Z. X. Wu, D. Feng, B. Tu and D. Y. Zhao, *J. Phys. Chem. C*, 2010, 114, 5012-5019.
39. Q. Li, Z. X. Wu, D. Feng, B. Tu and D. Y. Zhao, *J. Phys. Chem. C*, 2010, 114, 5012-5019.
40. A. B. Jarzçbski, J. Lorenc and L. Pająk, *Langmuir*, 1997, 13, 1280-1285.
41. C. J. Brinker and G. W. Scherer, *Sol-gel science : the physics and chemistry of sol-gel processing*, Academic Press, Boston, 1990.
42. D. W. Schaefer, *MRS Bull.*, 1988, 13, 22-27.

